NASA/CR-2008-215340
NESC-RP-08-09/06-081-E

Elastic-Plastic Fracture Mechanics Analysis of Critical Flaw Size in ARES I-X Flange-to-Skin Welds

G. Graham Chell and Stephen J. Hudak, Jr.
Southwest Research Institute, San Antonio, Texas

September 2008

The NASA STI Program Office . . . in Profile

Since its founding, NASA has been dedicated to the advancement of aeronautics and space science. The NASA Scientific and Technical Information (STI) Program Office plays a key part in helping NASA maintain this important role.

The NASA STI Program Office is operated by Langley Research Center, the lead center for NASA's scientific and technical information. The NASA STI Program Office provides access to the NASA STI Database, the largest collection of aeronautical and space science STI in the world. The Program Office is also NASA's institutional mechanism for disseminating the results of its research and development activities. These results are published by NASA in the NASA STI Report Series, which includes the following report types:

- TECHNICAL PUBLICATION. Reports of completed research or a major significant phase of research that present the results of NASA programs and include extensive data or theoretical analysis. Includes compilations of significant scientific and technical data and information deemed to be of continuing reference value. NASA counterpart of peer-reviewed formal professional papers, but having less stringent limitations on manuscript length and extent of graphic presentations.

- TECHNICAL MEMORANDUM. Scientific and technical findings that are preliminary or of specialized interest, e.g., quick release reports, working papers, and bibliographies that contain minimal annotation. Does not contain extensive analysis.

- CONTRACTOR REPORT. Scientific and technical findings by NASA-sponsored contractors and grantees.

- CONFERENCE PUBLICATION. Collected papers from scientific and technical conferences, symposia, seminars, or other meetings sponsored or co-sponsored by NASA.

- SPECIAL PUBLICATION. Scientific, technical, or historical information from NASA programs, projects, and missions, often concerned with subjects having substantial public interest.

- TECHNICAL TRANSLATION. English-language translations of foreign scientific and technical material pertinent to NASA's mission.

Specialized services that complement the STI Program Office's diverse offerings include creating custom thesauri, building customized databases, organizing and publishing research results ... even providing videos.

For more information about the NASA STI Program Office, see the following:

- Access the NASA STI Program Home Page at ***http://www.sti.nasa.gov***

- E-mail your question via the Internet to help@sti.nasa.gov

- Fax your question to the NASA STI Help Desk at (301) 621-0134

- Phone the NASA STI Help Desk at (301) 621-0390

- Write to:
  NASA STI Help Desk
  NASA Center for AeroSpace Information
  7115 Standard Drive
  Hanover, MD 21076-1320

NASA/CR-2008-215340
NESC-RP-08-09/06-081-E

Elastic-Plastic Fracture Mechanics Analysis of Critical Flaw Size in ARES I-X Flange-to-Skin Welds

G. Graham Chell and Stephen J. Hudak, Jr.
Southwest Research Institute, San Antonio, Texas

NASA Engineering and Safety Center
Langley Research Center
Hampton, Virginia 23681-2199

Prepared for the NASA Engineering and Safety Center under NASA contract NNL07AA00B

September 2008

Available from:

NASA Center for AeroSpace Information (CASI)
7115 Standard Drive
Hanover, MD 21076-1320
(301) 621-0390

Elastic-Plastic Fracture Mechanics Analysis of Critical Flaw Size in ARES I-X Flange-to-Skin Welds

G. Graham Chell and Stephen J. Hudak, Jr.
Southwest Research Institute®
San Antonio, TX

Abstract

NASA's ARES 1 Upper Stage Simulator (USS) is being fabricated from welded A516 steel. In order to insure the structural integrity of these welds it is of interest to calculate the critical *initial* flaw size (CIFS) to establish rational inspection requirements. The CIFS is in turn dependent on the critical *final* flaw size (CFS), as well as fatigue flaw growth resulting from transportation, handling and service-induced loading. Independent CFS, fatigue flaw growth and CIFS calculations for weld flaws in the flange-to-skin weld of the ARES I USS have been reported in a companion report. These calculations were made using linear elastic fracture mechanics (LEFM), which are thought to be conservative because they are based on a lower bound, so-called "elastic," fracture toughness determined from tests that displayed significant plasticity. Nevertheless, there was still concern that the yield magnitude stresses generated in the flange-to-skin weld by the combination of axial stresses due to axial forces, fit-up stresses, and weld residual stresses, could give rise to significant flaw-tip plasticity, which might render the LEFM results to be non-conservative.

Flaw-tip plasticity enhances flaw-tip "driving forces" compared to the values determined from LEFM. In fracture toughness tests that involve non-linear load-displacement behavior due to flaw-tip plasticity, this means that an elastic toughness value estimated using LEFM and the measured load and flaw depth will under-estimate the actual toughness as this approach is equivalent to determining the "driving force" using only the area under the linear part of the load-displacement curve. The actual toughness is related to the total area under the load-displacement curve including the non-linear part arising from flaw-tip plasticity. Hence, an elastically estimated toughness will always be lower than the actual value when non-linear behavior is observed in a toughness test. Similarly, flaw-tip "driving forces" for flaws in structures that are evaluated using LEFM concepts will under-estimate the actual "driving forces" when flaw-tip plasticity is present. Thus, the LEFM approach will only be conservative if the ratio of the "elastic" toughness, $K_C^{elastic}$ to the elastic-plastic toughness, $K_C^{elastic-plastic}$) is less than the ratio of the linear elastic flaw-tip "driving force" in the structure ($K = K^{elastic}$) to the elastic-plastic flaw-tip "driving force" ($K_J = K^{elastic-plastic}$).

The objective of the present study was to employ Elastic–Plastic Fracture Mechanics (EPFM) to determine CFS values, and then compare these values to CFS values evaluated using LEFM. CFS values were calculated for twelve cases involving surface and embedded flaws, EPFM

analyses with and without plastic shakedown of the stresses, LEFM analyses, and various welding residual stress distributions. For the cases examined, the computed CFS values based on elastic analyses were the smallest in all instances where the failures were predicted to be controlled by the fracture toughness. However, in certain cases, the CFS values predicted by the elastic-plastic analyses were smaller than those predicted by the elastic analyses; in these cases the failure criteria were determined by a breakdown in stress intensity factor validity limits for deep flaws ($a > 0.90t$), rather than by the fracture toughness. Plastic relaxation of stresses accompanying shakedown always increases the calculated CFS values compared to the CFS values determined without shakedown. Thus, it is conservative to ignore shakedown effects.

Table of Contents

Executive Summary

Independent critical flaw size calculations (CFS) for weld flaws in the flange-to-skin weld of the ARES I-X Upper Stage Simulator (USS) have been reported in Ref. 1. These calculations were made using linear elastic fracture mechanics (LEFM). Although the LEFM CFS evaluations are considered conservative because they are based on a lower bound, so-called "elastic," fracture toughness determined from tests that displayed significant plasticity, there is still concern that the yield magnitude stresses generated in the flange-to-skin weld by the combination of axial stresses due to axial forces, fit-up stresses, and weld residual stresses, could give rise to significant flaw-tip plasticity and a corresponding increase in the calculated flaw-tip "driving force" that could more than compensate for the conservatisms built into the LEFM approach.

A series of CFS computations were performed using an R&D version of the elastic-plastic fracture mechanics (EPFM) computer program FlawPRO™ developed by SwRI® for structural integrity assessments of welded steel pipe employed in the oil and gas industry. These calculations were made in order to assess whether or not the elastic approach adopted in Ref. 1 is conservative with respect to a more complex but technically more rigorous and consistent approach based on EPFM. This demonstration is necessary because although the elastic approach uses an "elastic" toughness which is significantly below the measured toughness (62 ksi inch$^{1/2}$ compared to 154 ksi inch$^{1/2}$) it is known that LEFM can under-predict flaw-tip "driving forces" compared to more accurate values determined using EPFM. Under certain conditions, it is possible that the under-prediction of the flaw-tip "driving force" based on LEFM analysis can more than compensate for the use of a low "elastic" toughness, thereby resulting in a non-conservative CFS value.

The CFS computations were made for surface and embedded flaws either at or near to the ID or OD of the flange-to-skin weld in A516 steel. Analyses were performed with axial and fit-up stresses superposed on four types of residual stresses. Unlike the elastic calculations, the elastic-plastic approach requires the applied stresses to be resolved into primary and secondary (residual stress) components. The weld residual stresses considered in the present assessment are:

- A uniform stress equal to the yield stress
- A stress consistent with a Double-V weld process
- A stress consistent with a 7 pass weld procedure with the last pass on the ID
- A stress consistent with a 7 pass weld procedure with the last pass on the OD

CFS computations using the elastic and elastic-plastic approaches showed that the predicted CFS's for surface flaws were significantly smaller than the CFS for embedded flaws. These computations also showed that the uniform and 7 pass (ID last) residual stresses were the most onerous of the four and resulted in the smallest CFS values. These stresses are so severe that when they are combined with those due to axial and fit-up stresses the resulting through-wall stresses exceed the yield stress. In actuality, plastic relaxation of stresses that exceed yield will occur, resulting in so-called shakedown and a reduction in the residual stresses. This shakedown phenomenon can be allowed for in elastic-plastic computations performed by FlawPRO. Shakedown is assumed not to occur in the elastic approach.

A summary of the CFS results for surface flaws is shown in Figure 1.

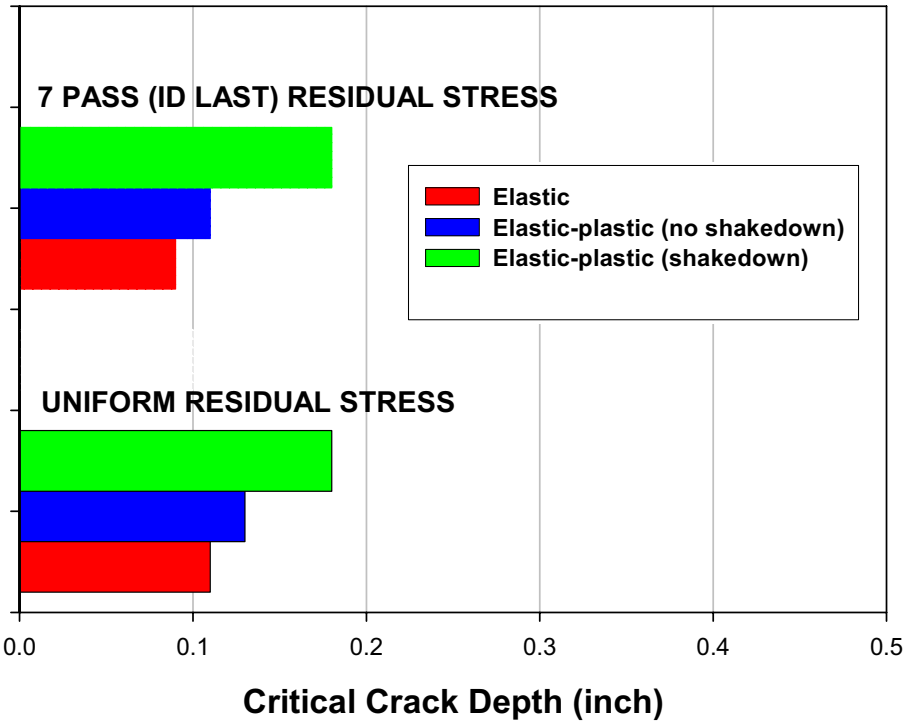

Figure 1. Summary of CFS values for surface flaws determined using elastic and elastic-plastic approaches, the latter with and without shakedown in residual stresses.

It is concluded from Figure 1 that CFS calculated for the most critical case of surface flaws using the elastic approach and a toughness of 62 ksi inch$^{1/2}$ will be smaller, and hence more conservative, than values computed using an elastic-plastic approach based on a toughness of 154 ksi inch$^{1/2}$, even if the potentially beneficial phenomenon of stress relaxation from shakedown is ignored. The same is not always true for embedded flaws; however, these cases give larger computed CFS values than for surface flaws using both elastic and elastic-plastic analyses, and thus are of less concern provided the surface flaw critical initial flaw size (CIFS) results are used to set weld defect acceptance limits.

Introduction

Independent critical flaw size calculations (CFS) for weld flaws in the flange-to-skin weld of the ARES I-X Upper Stage Simulator (USS) have been reported in Ref. 1. These calculations were made using linear elastic fracture mechanics (LEFM). Although the LEFM CFS evaluations are considered conservative because they are based on a lower bound, so-called "elastic," fracture toughness determined from tests that displayed significant plasticity, there is still concern that the yield magnitude stresses generated in the flange-to-skin weld by the combination of axial stresses due to axial forces, fit-up stresses, and weld residual stresses, could give rise to significant flaw-tip plasticity (i.e., a large plastic zone at the flaw tip compared to other relevant dimensions of the component – flaw size, unflawed ligament size) and a corresponding increase in the calculated flaw-tip "driving force" that could more than compensate for the conservatisms built into the LEFM approach.

Flaw-tip plasticity enhances flaw-tip "driving forces" compared to the values determined from LEFM. In fracture toughness tests that involve non-linear load-displacement behavior due to flaw-tip plasticity, this means that an elastic toughness value estimated using LEFM and the measured load and flaw depth will under-estimate the actual toughness as this approach is equivalent to determining the toughnesses using only the area under the linear part of the load-displacement curve. The actual toughness is related to the total area under the load-displacement curve including the non-linear part arising from flaw-tip plasticity. Hence, an elastically estimated toughness will always be lower than the actual value when non-linear behavior is observed in a toughness test. Similarly, flaw-tip "driving forces" for flaws in structures that are evaluated using LEFM concepts will under-estimate the actual "driving forces" when flaw-tip plasticity is present.

The LEFM approach adopted in Ref. 1 will be conservative if the ratio of the linear elastically determined flaw-tip "driving force" at fracture measured in a fracture toughness test (the elastic toughness, $K_C^{elastic}$) to the actual toughness (the elastic-plastic toughness, $K_C^{elastic-plastic}$) is less than the ratio of the linear elastic flaw-tip "driving force" in the structure ($K = K^{elastic}$) to the elastic-plastic flaw-tip "driving force" ($K_J = K^{elastic-plastic}$). This condition is expressed mathematically below:

$$\frac{K_C^{elastic}}{K_C^{elastic-plastic}} < \frac{K}{K_J}, \text{ LEFM approach is conservative} \qquad (1a)$$

$$\frac{K_C^{elastic}}{K_C^{elastic-plastic}} > \frac{K}{K_J}, \text{ LEFM approach is non-conservative.} \qquad (1b)$$

In these equations, the symbol *K* represents a flaw-tip "driving force" which has the units of stress intensity factor, and the subscripts and superscripts indicate whether the parameter is estimated using LEFM or elastic-plastic fracture mechanics (EPFM). The subscript *J* signifies a

quantity determined from the EPFM parameter, *J*. This parameter represents an extension of linear elastic concepts to cases involving flaw-tip plasticity. As such, *J* is related to *K* under linear elastic conditions. In general, *J* can be converted into a plastically corrected value of *K*, symbolized by K_J, using the equation:

$$J = \frac{K_J^2}{E'} \tag{2}$$

where $E' = E$, Young's modulus, for plane stress and $\frac{E}{\left(1-\nu^2\right)}$, for plane strain. (A similar equation to Eq. 2 is used to relate the toughness, J_C, measured in terms of J, in a test that exhibits significant flaw-tip plasticity to the toughness, $K^{elastic-plastic}$, expressed in units of stress intensity factor.)

Under LEFM conditions, Eq. 2 becomes

$$J_e = \frac{K^2}{E'} \tag{3}$$

and it is clear from Eqs. 2 and 3 that $K_J = K$ when these conditions are appropriate.

In the present study, EPFM is used to determine CFS's and these sizes are compared to CFS's evaluated using LEFM. Eq. 1a is equivalent to the inequality CFS(LEFM) < CFS(EPFM) and 1b to the inequality CFS(LEFM) > CFS(EPFM), where the nomenclature is self-explanatory.

Estimating J Using EPFM

Although *J* can be evaluated from elastic-plastic finite element analyses of flawed structures, this is often not practical because of time and cost constraints. To overcome this obstacle, analytical schemes have been developed for determining *J* based on quantities such as the LEFM parameter, *K*, the local stresses due to applied forces and moments, the values of the forces and moments that result in net section yielding (where the un-flawed ligament is everywhere at the yield stress), and the material stress-strain curve. In these schemes, *J* is expressed as the sum of an elastic component, J_e, and a plastic component, J_p, as illustrated in the Eq. 4:

$$J(a,F) = J_e(a_e,F,\sigma_y) + J_p(a,F,F_y,\sigma-\varepsilon) \tag{4}$$

In this equation, *a* is the flaw depth, *F* is the applied force, σ_y is the yield stress, a_e is a first order plastic correction to the actual flaw depth evaluated according to an Irwin type of plastic-zone equation, F_y is the net section yield force, and $\sigma-\varepsilon$ signifies the stress-strain curve. Eq. 4 is consistent with the *J* estimation scheme developed by GE for the Electric Power Research Institute (EPRI) based on extensive finite element computations of *J*, and is generally referred to as the GE/EPRI scheme, see Ref. 2.

In the present work, J is formulated using a hybrid scheme that employs the form of Eq. 4 with the first term on the right-hand side of the equation determined according to the GE/EPRI scheme, but with the plastic component determined according to the reference stress approach developed in Ref. 3. The reference stress approach provides the theoretical framework underpinning two widely employed fitness-for-service assessment procedures, namely API 579 (Ref. 4) and BS 7910 (Ref. 5).

Failure Criteria

In the LEFM approach, failure is predicted when the following equation is satisfied:

$$K \geq K_C^{elastic} \tag{5a}$$

In the EPFM approach, failure is predicted when:

$$K_J = \sqrt{E' J} \geq \sqrt{E' J_C} = K_C^{elastic-plastic} \tag{5b}$$

such that

$$K_J \geq K_C^{elastic-plastic} \tag{5c}$$

Eqs. 5 represent failure when materials are brittle. In these cases, failure under monotonic loading conditions is usually catastrophic and not preceded by stable flaw extension. However, in some materials, such as those steels used in the flange-to-skin weld, the toughness, J_C, coincides with the onset of stable flaw extension, not catastrophic failure. These ductile steels display increasing toughness as a flaw extends (tears) under increasing monotonic load. The present analysis takes no account of the enhanced toughness (J-R curve) due to the material's ductility, and hence the results are conservative with respect to the results of an analysis that includes these beneficial effects.

Furthermore, the current calculations do not explicitly account for plastic constraint effects on failure behavior. It is known that under some circumstances, constraint effects related to loss of tri-axial stress conditions at a loaded flaw-tip can result in higher measured toughness (J_C) values (when these are determined in terms of the conventional formulations for J related to the area under a load-displacement curve) than those measured in test specimens where full tri-axial stress states pertain, such as deep flaws in bend bars under small scale yielding (small plastic zone) conditions. (Under full tri-axial stressing, the parameter J characterizes the magnitudes of the stresses and strains adjacent to a flaw tip and can be related to the failure mechanisms activated by these. When full tri-axial stressing is not attained, the relationship between J and the flaw-tip fields, and hence the failure mechanisms, is more complicated, involving additional stress parameters not directly related to J, and so the critical value of J, J_C, measured at failure no longer appears to be a true material constant.) In the present calculations, it is assumed that constraint effects are included in the measured fracture toughness and so they are not included in the flaw-tip "driving force", J.

CFS's are determined by solving Eqs. 5a and 5b for the flaw height, h, for given flaw length, L, applied forces, and local stresses. For surface flaws $h = a$, the flaw depth, and $L = 2c$, where c is half the flaw length. In the case of embedded flaws, $h = 2a$ and $L = 2c$.

Computations of CFS's were performed in the current work using an R&D version of the computer program FlawPRO^{TM} developed by SwRI for the offshore oil and gas industry. This program is based on EPFM and uses the hybrid J estimation scheme together with the failure criterion given in Eq. 5b. FlawPRO is also used to perform LEFM CFS calculations by making the input value of the material yield stress very high so that flaw-tip plasticity is suppressed and by setting the fracture toughness to the elastic value. With these modifications, the failure criterion represented by Eq. 5a is recovered from Eq. 5b.

FlawPRO has a number of additional failure criteria that are not related to fracture toughness and are applied in parallel with Eq. 5b. These additional criteria are designed to guarantee a conservative CFS is obtained for cases where the actual CFS is predicted to exceed the maximum flaw sizes corresponding to the geometrical limits of the available stress intensity factor (SIF) solutions. Typically, the SIF solutions are applicable to flaw heights less than 90% of the wall thickness (t). If the critical flaw height, h_{crit}, is predicted to exceed $0.9t$, then h_{crit} is set equal to $0.9t$. However, the J estimation scheme given by Eq. 4 involves the first order plastically corrected flaw height, h_e. This term will always exceed h since $h_e = h + s$ where the size of s is related to the size of the flaw-tip plastic zone as predicted from first order plasticity theory. If the value of h_e during the search for the critical height is predicted by FlawPRO to exceed $0.9t$, then h_{crit} is set equal to $0.9t$-s.

These additional geometrical failure criteria in FlawPRO dictated by restrictions imposed by SIF solution limits are summarized in Eqs. 6a and 6b.

$$h_{crit} = 0.9t \text{ if } h_{crit} \text{ predicted to exceed } 0.9t \tag{6a}$$

$$h_{crit} = 0.9t - s \text{ if } h_e \text{ corresponding to } h_{crit} \text{ predicted to exceed } 0.9t \tag{6b}$$

Assumptions Made and Input Data Used in the CFS Calculations

As previously mentioned, all CFS calculations reported in this study were determined using FlawPRO.

The flange-to-skin weld is subjected to three sources of loading: an axial force (Ref. 6), fit-up stresses (Ref. 6), and weld residual stresses (Ref. 7). It is necessary in EPFM calculations to separate the applied loads into primary and secondary components as these are treated differently within the hybrid J scheme. The axial load applied to the flange-to-skin weld is a primary load. The fit-up stresses arise from a complex set of boundary conditions which make them very difficult to categorize as purely secondary or purely primary. Because of this, and the fact that the fit-up stresses integrate to produce a net force on the weld, these stresses are conservatively treated as originating from a primary load. The weld residual stress is an example of a secondary

load. The total of primary and secondary stresses is included in the evaluation of J_e in Eq. 4 but only the primary stresses are included in the evaluation of J_p.

Four different assumptions were made herein regarding the form of the local stress variations through the wall of the flange-to-skin weld. In all cases, these assumptions affected the form of the residual stress variation but not the form of the axial and fit-up stresses. The four types of residual stress variations considered were:

1. A uniform variation through the wall of the skin equal to the yield stress.

2. A through-wall variable stress determined from a finite element simulation of the welding procedure for a Double-V weld, as described in Ref. 7. This stress is hereafter referred to as the Double-V residual stress.

3. A through-wall variable stress determined from a finite element simulation of the welding procedure based on a 7 pass process with the last pass at the ID, as described in Ref. 7. This stress is hereafter referred to as the 7 Pass (ID Last) residual stress.

4. A through-wall variable stress determined from a finite element simulation of the welding procedure based on a 7 pass process with the last pass at the OD, as described in Ref. 7. This stress is hereafter referred to as the 7 Pass (OD Last) residual stress.

If the sum of the residual stress and the axial and fit-up stresses is less than the yield stress at every point through the wall of the skin, then the residual stress would be unchanged when the axial and fit-up stresses were superposed on it. However, if the sum of the stresses exceeds the yield stress, then shakedown (stress relaxation due to plasticity) of the residual stress will occur, changing the residual stress variation determined absent the axial and fit-up stresses. All stress relaxation is herein assumed to occur in the residual stress (which is nearly self-equilibrated). The primary (axial and fit-up) stresses are assumed unchanged after shakedown because when integrated through the wall they must still produce the total force applied before shakedown which is equal to the original axial force and the force resulting from fit-up stresses, thus no plastic relaxation can occur.

In the present work, shakedown in the residual stress is predicted to occur. In order to assess the significance of shakedown, CFS calculations were performed using the uniform, Double-V, 7 Pass (ID Last) and 7 Pass (OD Last) residual stresses before (absent shakedown) and after shakedown. Shakedown was not considered in the elastic CFS analyses as in these types of analyses it is inherently assumed that the material has an infinite yield stress, thus no plastic relaxation can occur.

The axial, fit-up, and residual stresses used in the CFS calculations absent shakedown are shown in Figures 2(a), 3(a), 4(a) and 5(a) for the uniform, Double-V, 7 Pass (ID Last) and 7 Pass (OD Last) residual stresses, respectively. The combined axial and fit-up stresses shown in these figures are consistent with the axial and fit-up stresses detailed in Ref. 6. The residual stresses after shakedown, corresponding to those shown in Figures 2(a), 3(a), 4(a) and 5(a), are displayed in Figures 2(b), 3(b), 4(b) and 5(b) for the uniform, Double-V, 7 Pass (ID Last) and 7 Pass (OD

Last) residual stresses, respectively. As previously mentioned, the axial and fit-up stresses are assumed unaffected by shakedown. The shakedown analysis incorporated in FlawPRO was used to obtain the results in Figures 2(b), 3(b), 4(b) and 5(b). The procedure used in this program to convert an elastically determined stress variation into a corresponding elastic-plastic variation is based on the Neuber principle.

The stress variations (stress versus x/t, where t is the wall thickness and x the distance from the origin) shown in Figures 2 through 5 were input in FlawPRO when performing CFS evaluations. The axial and fit-up stresses are input in normalized form (local stress/nominal stress) where the nominal stress is the value of the axial and fit-up stresses averaged through the wall of the skin. The average or nominal stress value is 16.2 ksi for the axial and fit-up stresses shown in Figures 2 through 5.

The total applied force, F, is required in the current approach as J_p involves determination of the ratio F/F_y. The value of F was determined by integrating the axial and fit-up stresses through the skin wall. This force corresponds to a nominal axial stress of 16.2 ksi.

The complex geometry of the skin, flange, flange-to-skin weld and the gussets were treated as a cylinder with OD equal to 216 inches and wall thickness of 0.5 inches. In the CFS calculations, circumferential surface flaws were either assumed to emanate from the ID or the OD of the cylinder, depending on the assumed form of the weld residual stresses. For example, flaws emanating from the ID are subjected to more severe stressing than those emanating from the OD if the weld residual stresses are assumed to have a uniform value through the wall of the skin or to be generated using the 7 Pass (ID Last) procedures, as shown in Figures 2 and 4, respectively. In this case the assumption is made in the CFS calculations that there are ID weld flaws. In contrast, flaws emanating from the OD were considered more onerous than those emanating from the ID if the weld residual stresses are assumed to be due to the Double-V and 7 Pass (OD Last) procedures, as shown in Figures 3 and 5, respectively.

A key parameter in both the EPFM and LEFM CFS calculations is the stress intensity factor, K. This is determined for surface and embedded flaws in FlawPRO using the weight function method. This is a powerful method that allows for through-the-wall stress variations based on stresses determined from a flaw-free stress analysis. It is not necessary to resolve stresses into primary and secondary components when using the weight function approach.

Stress-strain data are required to implement the EPFM methodology in FlawPRO. In the CFS calculations, it is conservative to use the stress-strain curve corresponding to the parent material even though the flaws are assumed to occur in the weld because the yield stress of the parent is less than that of the weld since the weld is overmatched. Examples of measured stress-strain curves for parent material are shown in Figure 6(a). These curves identify specimen 10240-1F as having the lowest yield stress. The curve corresponding to this specimen was used in the CFS calculations and Figure 6(b) compares the measured curve with the curve used as input to FlawPRO.

Results of CFS Calculations

Overview

A total of thirty-three sets of CFS calculations were performed. Six of the calculation sets were carried out to study the sensitivity of the elastic-plastic results to toughness. The cases are listed in Table 1. Details of the results for the thirty-three cases are given in Tables 2 through 10 and Figures 7 through 15. Table 1 identifies which tables and figures are applicable to each set of CFS calculations.

The majority of the EPFM calculations were performed using a fracture toughness of 154 ksi inch$^{1/2}$ and are referred to as the baseline computations. In addition, as part of the sensitivity study, four further sets of EPFM CFS computations were made: two for surface flaws assuming toughness of 115 ksi inch$^{1/2}$ and 62 ksi inch$^{1/2}$, and two for offset embedded flaws assuming toughness values in the range 40-120 ksi inch$^{1/2}$. All the LEFM computations were made assuming an "elastic" toughness of 62 ksi inch$^{1/2}$ and form part of the baseline calculations.

Two types of embedded flaws were considered in the CFS calculations. These were offset and center flaws. Offset embedded flaws were assumed offset 0.07874 inch (2 mm) from the ID or OD, where the offset is the distance between the ID or OD surface and the nearest point on the flaw. The centers of these types of flaws are located at distances from the ID or OD surfaces equal to the offsets (y) plus half the flaw heights (a). Center embedded flaws were assumed to have their centers located at the mid-wall.

Non-toughness-based failure criteria, specifically fully-plastic limit loads, were used to determine some of the critical flaw heights listed in Tables 2 through 10. These criteria are related to the maximum flaw size limits of the available weight functions used in the K calculations, as shown in Eqs. 6a and 6b. The non-toughness based critical flaw heights are indicated in the tables by asterisks. These values represent lower bound (conservative) estimates for critical flaw heights compared to values derived using the toughness based failure criteria shown in Eqs. 5a and 5b.

Baseline results

Consider first surface flaws emanating from the ID subject to the axial and fit-up stresses superposed on a uniform residual stress. The elastic-plastic results without and with shakedown, and the elastic results without shakedown, are shown in Table 2 and Figure 7. In these cases, the calculated elastic CFS's are the smallest with the limiting CFS for very long flaw lengths being 0.11 inches compared to 0.13 inches for the elastic-plastic analysis without shakedown and 0.18 inches for the elastic-plastic analysis with shakedown. Since shakedown reduces the residual stress, CFS values calculated without shakedown will always be smaller than those with shakedown.

The offset embedded flaw results for the case of a uniform residual stress are shown in Table 3 and Figure 8. The smallest calculated CFS for very long flaws is predicted to be 0.23 inches and corresponds to an elastic-plastic analysis without shakedown. However, this size is a conservative estimate since it was obtained using a non-toughness related failure criterion, as indicated in Table 3. The linear elastic CFS result for long flaws is slightly larger at 0.29 inches, and the elastic-plastic result with shakedown is 0.35 inches. The reason that the elastic-plastic CFS without shakedown is less than the elastic result is because the failure condition represented by Eq. 6b was operative in FlawPRO for this case, whereas the failure condition represented by Eq. 5a was applicable in the elastic computations.

Next consider the CFS results for surface flaws emanating from the OD subject to the axial and fit-up stresses superposed on the Double-V residual stress. The elastic-plastic results without and with shakedown, and the elastic results without shakedown, are shown in Table 4 and Figure 9. For these cases, the smallest CFS's correspond to the elastic-plastic analysis without shakedown and the elastic analysis, and for very long flaw lengths are equal to 0.25 inches, compared to 0.26 inches for the elastic-plastic analysis with shakedown. These critical values are all based on the toughness based failure criterion.

Center and offset embedded flaw results for the Double-V residual stress are displayed in Tables 5 and 6 and Figures 10(a) and (b), respectively. In this residual stress case, center embedded flaws were analyzed as well as offset embedded flaws because the no shakedown and shakedown stress variations are approximately symmetrical and achieve maximum values at about the mid-wall ($x/t = 0.5$), as can be seen in Figure 3. The results in Tables 5 and 6 illustrate that for both types of embedded flaws, and for all three types of analyses, the critical flaw heights were determined based on conservative non-toughness related failure criteria. This is because the flaw-tip "driving forces" corresponding to embedded flaws are considerably smaller than the flaw-tip "driving forces", for surface flaws with the same flaw heights, and can only attain values equal to the toughness at very large sizes. The critical heights for the offset flaws are smaller than those for the center flaws, and both sets of values are large (greater than 0.38 inch) compared to the wall thickness of 0.5 inch.

Tables 7 and 8, and Figures 11 and 12 contain CFS for surface and offset embedded flaws subjected to residual stresses generated by the 7 Pass (ID Last) weld procedure. The smallest CFS corresponding to surface flaws is predicted from an elastic analysis to be 0.09 inch. This value compares with the 0.11 inch and 0.18 inch predictions obtained from elastic-plastic analyses based on no shakedown and shakedown, respectively. These relatively small CFS values reflect the high stresses experienced by surface flaws emanating from the ID (see Figure 4). The corresponding CFS values for embedded flaws are significantly higher. Although, in these cases, the smallest CFS value of 0.2 inch is predicted from an elastic-plastic analysis assuming no shakedown, this value is conservatively small and was determined using a failure criterion related to the K solution geometrical validity limits. The smallest elastically calculated CFS is 0.28 inch and is derived when the flaw-tip "driving force" exceeds the toughness.

Tables 9 and 10, and Figures 13 and 14 contain CFS for surface and offset embedded flaws emanating from the OD that experience residual stresses generated by the 7 Pass (OD Last) weld

process. In these cases, the smallest CFS of 0.2 inch is predicted by the elastic analysis of a surface flaw. This value compares with predicted values of 0.21 inch and 0.23 inch obtained from elastic-plastic analyses based on no shakedown and shakedown, respectively. All of the CFS results for embedded flaws are determined from non-toughness related failure criteria, and all are very large (0.4 inch).

Toughness sensitivity studies

A limited study was performed to investigate the dependence of predicted EPFM CFS with toughness. This study concentrated on toughness values that were low enough to guarantee toughness controlled failures. The calculations were performed for long flaws with a constant aspect ratio (*a/2c = 0.005* for surface and *h/2c = 0.005* for embedded flaws) as these result in the lowest CFS values.

Table 2 and Figure 7, and Table 7 and Figure 11, present EPFM surface CFS results for toughness values of 115 ksi inch$^{1/2}$ and 62 ksi inch$^{1/2}$ as well as for 154 ksi inch$^{1/2}$ in order to assess the sensitivity of the CFS values to toughness. These calculations were performed assuming no shakedown, one with a uniform residual stress of 46.5 ksi and the other the residual stress signified as 7 Pass (ID last). These two types of residual stress were considered the severest of the cases considered as they resulted in the smallest CFS values.

The results in Figures 7 and 11 demonstrate that the EPFM surface CFS values for a toughness of 62 ksi inch$^{1/2}$ for the uniform and 7 Pass (ID Last) residual stresses, respectively, are both lower than the elastic values for the same toughness. This is not surprising because, as previously stated, the EPFM "driving force" will always exceed the elastic force. However, in both residual stress cases, the CFS values determined using a toughness of 115 ksi inch$^{1/2}$ exceed those calculated from an elastic analysis for a toughness of 62 ksi inch$^{1/2}$. Therefore, for surface flaws subjected to the severest residual stresses, the assumption that the elastic CFS solutions based on a toughness of 62 ksi inch$^{1/2}$ are conservative with respect to an EPFM analysis based on a toughness of 154 ksi inch$^{1/2}$ is readily justified by the current results.

The sensitivity of the EPFM embedded CFS to fracture toughness was also investigated for the uniform and 7 Pass (ID Last) residual stresses with and without shakedown. Toughness values in the range 60 ksi inch$^{1/2}$ to 120 ksi inch$^{1/2}$ were considered in the calculations that did not include shakedown as these resulted in toughness controlled failures. The failure criterion switched from toughness controlled to non-toughness controlled for values higher than 115 ksi inch$^{1/2}$ for the uniform residual stress, and 120 ksi inch$^{1/2}$ for the 7 Pass (ID Last) stress. Toughness values in the range 40 ksi inch$^{1/2}$ to 90 ksi inch$^{1/2}$ were considered in the calculations that included shakedown as these resulted in toughness controlled failures. The failure criterion changed from toughness controlled to non-toughness controlled for values higher than 90 ksi inch$^{1/2}$ for the uniform residual stress, and 50 ksi inch$^{1/2}$ for the 7 Pass (ID Last) stress. In all cases, the predicted failures were found to be governed by the size of the first order plastically corrected flaw height (see Eq. 6b).

The results of this sensitivity study are displayed in Figure 15 as a plot of critical flaw height against toughness. Also shown in this figure are the elastic results for the two residual stresses.

It can be seen that in contrast to the surface flaw CFS solutions when it was assumed there was no shakedown, the predicted EPFM critical flaw sizes for offset embedded flaws are lower than the elastically determined values for toughness values up to 120 ksi inch$^{1/2}$(compare Figures 7 and 11 with Figure 15). Indeed, simple extrapolation of the critical flaw height results in Figure 15 to toughness values of 154 ksi inch$^{1/2}$ indicates that even at this toughness level the EPFM results for the embedded flaws could be lower than the elastic values, which are around 0.28 inch.

In contrast to the no shakedown case, when shakedown is assumed to reduce the residual stress level, the CFS values are relatively large at small toughness values for both types of residual stress (see Figure 15). The EPFM toughness controlled embedded CFS values are larger than the elastic value for toughness values greater than 65 ksi inch$^{1/2}$ in the case of the uniform residual stress. Although, at a toughness of 50 ksi inch$^{1/2}$ the EPFM embedded CFS values are below the elastic value for the 7 Pass (ID Last) residual stress, it is clear from the trend of CFS with toughness shown in Figure 15 that the EPFM values will exceed the elastic value at toughness values exceeding 60 ksi inch$^{1/2}$.

Discussion

Although the EPFM flaw-tip "driving force", J, is composed of elastic (first order plastic) and plastic components (see Eq. 4), the plastic term was always negligibly small in the present calculations compared to the elastic term. This is because this term depends on the ratio F/F_y which has a value of around 0.4 in the current computations. Usually, the plastic component of J does not start to become comparable to the elastic term until $F/F_y>1$. Thus it is the first order plastic correction (h_e) to the flaw height (h) and the resulting increase in $J(h_e)$ compared to the elastic parameter $J(h)$ that contributes most to the reduction in EPFM CFS values compared to the elastically determined values when the same toughness is used in both calculations.

Summary and Conclusions

CFS's have been calculated using the computer program FlawPRO for thirty-three cases involving surface and embedded flaws, elastic-plastic analyses (with and without shakedown), elastic analyses, four types of residual stresses, and a range of toughness values (used in a limited sensitivity study). Two types of baseline calculations were performed. In the first, EPFM computations were made using a toughness of 154 ksi inch$^{1/2}$. In the second, LEFM calculations were performed based on an "elastic" toughness of 62 ksi inch$^{1/2}$. In all the cases addressed, axial and fit-up stresses were superposed on the residual stresses.

The following conclusions are drawn from the results of the two baseline computations:

1. The lowest calculated critical flaw height was 0.09 inches corresponding to the elastic results for a very long surface flaw emanating from the ID subject to a residual stress signified as 7 Pass (ID Last) (see Table 7). Although determined for an assumed toughness of 62 ksi inch$^{1/2}$, this value is only slightly smaller than the critical height of 0.11 inches calculated using elastic-plastic fracture mechanics, a toughness of 154 ksi

inch$^{1/2}$, and ignoring the potential for shakedown of the residual stress. Allowing shakedown in the calculations results in an increase in critical height from 0.11 inches to 0.18 inches.

2. The next severest residual stress to the 7 Pass (ID Last) is a uniform residual stress equal to yield. The elastically calculated critical flaw height for this residual stress is 0.11 inches, which compares with elastic-plastic analysis results obtained assuming no shakedown and shakedown of 0.13 inches and 0.18 inches, respectively (see Table 2).

3. It was found in all the analyses performed that CFS values for surface flaws were smaller than those predicted for embedded flaws. The reason for this is that for the same applied stresses and flaw heights and lengths, embedded flaws have significantly smaller calculated flaw-tip "driving forces" than do surface flaws.

4. In many of the baseline calculations, the CFS's calculated by FlawPRO were not fracture toughness controlled failures as represented by Eqs. 5a and 5b but were determined instead by the failure criteria given in Eqs. 6a and 6b that are related to maximum flaw sizes corresponding to the geometrical validity limits of the SIF solutions available in the program.

5. The CFS's computed in the baseline studies using elastic analyses were the smallest in all cases where the failures were predicted to be controlled by the fracture toughness. In some cases, the CFS's predicted by the elastic-plastic analyses were smaller than those predicted by the elastic analyses, but in these baseline cases the failure criteria were determined by the maximum flaw size limits on the available K solutions rather than the fracture toughness.

6. Shakedown always increases the calculated CFS's compared to the CFS's determined without shakedown. Thus, it is conservative to ignore shakedown effects.

The following conclusions are drawn from the results of the toughness sensitivity computations made using the uniform and 7 Pass (ID Last) residual stresses with and without shakedown and assuming the flaws were long with aspect ratios of 0.005:

1. The EPFM surface CFS values are predicted to exceed the elastic values for toughness values greater than 115 ksi inch$^{1/2}$ when no shakedown is assumed. This result confirms that surface CFS determined elastically using a toughness of 62 ksi inch$^{1/2}$ will be conservative with respect to EPFM calculations based on a toughness of 154 ksi inch$^{1/2}$ whether or not shakedown is assumed.

2. It could not be demonstrated for the no shakedown cases that EPFM offset embedded CFS values obtained using a toughness of 154 ksi inch$^{1/2}$ would exceed the elastically calculated values based on a toughness of 62 ksi inch$^{1/2}$ and hence would be conservative.

3. It was demonstrated that if shakedown in the residual stress was accounted for, that EPFM offset embedded CFS values obtained using a toughness of 154 ksi inch$^{1/2}$ will be greater than the elastically calculated values based on a toughness of 62 ksi inch$^{1/2}$. In this case, elastic computations are conservative with respect to EPFM computations.

Acknowledgements

Many people contributed to the information and knowledge needed to complete the analysis summarized in this report: Derrick Cheston provided overall leadership and kept the team focused on the practical problem; Bob Piascik introduced us to the problem and provided guidance on materials issues and the importance of fit-up stress; and Curt Larsen estimated the Ares I-X USS loading histories. I. S. Raju provided overall technical guidance, and together with Norm Knight, provided the stress analysis results (Ref. 6). Fred "Bud" Brust provided the welding residual stress simulation results (Ref. 7); Dave Dawicke helped us with all the required input, including material properties, and also provided the results from the linear-elastic analysis (Ref. 1) for comparison with the current elastic-plastic analyses. Walter Reuter provided much useful discussion on constraint effects, and together with Roy Hampton, critically reviewed the initial manuscript.

References

1. Dawicke, D. S., Raju, I. S., and Cheston, D. J. "Critical Initial Flaw Size Analysis," NASA/TM-2008-215337, August 2008.

2. Kumar, M., German, D., and Shih, C. F., *An Engineering Approach for Elastic-Plastic Fracture Analysis*, EPRI Report NP-1931, Electric Power Research Institute, Palo Alto, CA, 1981.

3. Ainsworth, R. A., The Assessment of Defects in Structures of Strain Hardening Materials, *Eng. Fract. Mechanics,* Vol. 19, 1984, p. 633.

4. API 579, "Recommended Practice for Fitness-for-service," Washington D.C., American Petroleum Institute, 2000.

5. BS 7910:1999, "Guide on Methods for Assessing the Acceptability of Flaws in Fusion Welded Structures," British Standards Institute, 1999.

6. Knight, N., Phillips, D., and Raju, I. S., "Ares I-X USS Stress Analysis," NASA/TM-2008-215336, August 2008.

7. Brust, F., *et al* "Ares I-X USS Weld Residual Stress Analysis," NASA/TM-2008-215339, August 2008.

Table 1. ARES I-X critical flaw size calculations performed for parent material. Embedded flaws were either offset 0.07874 inch (2 mm) from the ID or OD, or located with their centers at mid-wall.

Flaw Type	Origin of Coordinates	Applicable Stresses	Toughness (ksi $in.^{1/2}$)	Results
ELASTIC-PLASTIC - UNIFORM RESIDUAL STRESS (46.5 ksi)				
Surface	ID surface	Membrane and Fit-up Residual (No shakedown) Figure 2(a)	154	Table 2 Figure 7
Offset Embedded	ID surface	Membrane and Fit-up Residual (No Shakedown) Figure 2(a)	154	Table 3 Figure 8
Surface*	ID surface	Membrane and Fit-up Residual (No shakedown) Figure 2(a)	115	Table 2 Figure 7
Surface*	ID surface	Membrane and Fit-up Residual (No shakedown) Figure 2(a)	62	Table 2 Figure 7
Surface	ID surface	Membrane and Fit-up Residual (After Shakedown) Figure 2(b)	154	Table 2 Figure 7
Offset Embedded	ID surface	Membrane and Fit-up Residual (After Shakedown) Figure 2(b)	154	Table 3 Figure 8
ELASTIC - UNIFORM RESIDUAL STRESS (46.5 ksi)				
Surface	ID surface	Membrane and Fit-up Residual (No Shakedown) Figure 2(a)	62	Table 2 Figure 7
Offset Embedded	ID surface	Membrane and Fit-up Residual (No Shakedown) Figure 2(a)	62	Table 3 Figure 8
ELASTIC-PLASTIC - DOUBLE-V RESIDUAL STRESS				
Surface	OD surface	Membrane and Fit-up Residual (No Shakedown) Figure 3(a)	154	Table 4 Figure 9
Center Embedded	OD surface	Membrane and Fit-up Residual (No Shakedown) Figure 3(a)	154	Table 5 Figure 10(a)
Offset Embedded	OD surface	Membrane and Fit-up Residual (No Shakedown) Figure 3(a)	154	Table 6 Figure 10(b)
Surface	OD surface	Membrane and Fit-up Residual (After Shakedown) Figure 3(b)	154	Table 4 Figure 9
Center Embedded	OD surface	Membrane and Fit-up Residual (After Shakedown) Figure 3(b)	154	Table 5 Figure 10(a)
Offset Embedded	OD surface	Membrane and Fit-up Residual (After Shakedown) Figure 3(b)	154	Table 6 Figure 10(b)
ELASTIC - DOUBLE-V RESIDUAL STRESS				
Surface	OD surface	Membrane and Fit-up Residual (No Shakedown) Figure 3(a)	62	Table 4 Figure 9
Center Embedded	OD surface	Membrane and Fit-up Residual (No Shakedown) Figure 3(a)	62	Table 5 Figure 10(a)
Offset Embedded	OD surface	Membrane and Fit-up Residual (No Shakedown) Figure 3(b)	62	Table 6 Figure 10(b)

* Toughness sensitivity study.

Table 1 (contd.). ARES I-X critical flaw size calculations performed for parent material.

Flaw Type	Origin of Coordinates	Applicable Stresses	Toughness (ksi in.$^{1/2}$)	Results
ELASTIC-PLASTIC - 7 PASS (ID LAST) RESIDUAL STRESS				
Surface	ID surface	Membrane and Fit-up Residual (No shakedown) Figure 4(a)	154	Table 7 Figure 11
Offset Embedded	ID surface	Membrane and Fit-up Residual (No Shakedown) Figure 4(a)	154	Table 8 Figure 12
Surface*	ID surface	Membrane and Fit-up Residual (No shakedown) Figure 4(a)	115	Table 7 Figure 11
Surface*	ID surface	Membrane and Fit-up Residual (No shakedown) Figure 4(a)	62	Table 7 Figure 11
Surface	ID surface	Membrane and Fit-up Residual (After Shakedown) Figure 4(b)	154	Table 7 Figure 11
Offset Embedded	ID surface	Membrane and Fit-up Residual (After Shakedown) Figure 4(b)	154	Table 8 Figure 12
ELASTIC - 7 PASS (ID LAST) RESIDUAL STRESS				
Surface	ID surface	Membrane and Fit-up Residual (No Shakedown) Figure 4(a)	62	Table 7 Figure 11
Offset Embedded	ID surface	Membrane and Fit-up Residual (No Shakedown) Figure 4(a)	62	Table 8 Figure 12
ELASTIC-PLASTIC - 7 PASS (OD LAST) RESIDUAL STRESS				
Surface	OD surface	Membrane and Fit-up Residual (No Shakedown) Figure 5(a)	154	Table 9 Figure 13
Offset Embedded	OD surface	Membrane and Fit-up Residual (No Shakedown) Figure 5(a)	154	Table 10 Figure 14
Surface	OD surface	Membrane and Fit-up Residual (After Shakedown) Figure 5(b)	154	Table 9 Figure 13
Offset Embedded	OD surface	Membrane and Fit-up Residual (After Shakedown) Figure 5(b)	154	Table 10 Figure 14
ELASTIC - 7 PASS (OD LAST) RESIDUAL STRESS				
Surface	OD surface	Membrane and Fit-up Residual (No Shakedown) Figure 5(a)	62	Table 9 Figure 13
Offset Embedded	OD surface	Membrane and Fit-up Residual (No Shakedown) Figure 5(a)	62	Table 5 Figure 14
ELASTIC-PLASTIC – UNIFORM and 7 PASS (ID LAST) RESIDUAL STRESS				
Offset Embedded*	ID surface	Membrane and Fit-up Residual (No Shakedown) Figure 2(a) and 4(a)	60-125	Figure 15
Offset Embedded*	ID surface	Membrane and Fit-up Residual (After Shakedown) Figure 2(b) and 4(b)	40-90	Figure 15

* Toughness sensitivity study.

Table 2. Critical flaw size results for surface flaws emanating from the ID: uniform residual.

Surface ID Flaw Uniform Residual Stress = 46.5 ksi									
Elastic-Plastic K_C = 154 ksi inch$^{1/2}$ (Shakedown)		Elastic-Plastic K_C = 154 ksi inch$^{1/2}$ (No Shakedown)		Elastic K_C = 62 ksi inch$^{1/2}$		Elastic-Plastic K_C = 115 ksi inch$^{1/2}$ (No Shakedown)		Elastic-Plastic K_C = 62 ksi inch$^{1/2}$ (No Shakedown)	
Flaw Height (in.)	Flaw Length (in.)	Flaw Height (in.)	Flaw Length (in.)	Flaw Height (in.)	Flaw Length (in.)	Flaw Height (in.)	Flaw Length (in.)	Flaw Height (in.)	Flaw Length (in.)
0.44*	0.44	0.43*	0.43	0.37	0.37	0.43*	0.43	0.24	0.24
0.42*	0.84	0.40*	0.80	0.27	0.53	0.40*	0.80	0.20	0.40
0.37*	1.49	0.32*	1.30	0.24	0.94	0.32*	1.30	0.17	0.68
0.36*	1.78	0.30*	1.51	0.20	1.00	0.30*	1.51	0.15	0.75
0.34*	2.05	0.28*	1.70	0.18	1.06	0.27	1.61	0.14	0.82
0.32*	2.52	0.26*	2.05	0.15	1.22	0.24	1.90	0.12	0.93
0.30*	3.01	0.24*	2.43	0.14	1.40	0.21	2.14	0.10	1.04
0.26*	5.22	0.18	3.52	0.12	2.37	0.15	2.91	0.08	1.60
0.19	18.66	0.13	12.98	0.11	10.96	0.11	11.23	0.07	6.78
0.18	36.52	0.13	25.30	0.11	21.78	0.11	22.00	0.07	13.43

* Critical height equals K solution geometrical validity limit based on first order plastically corrected flaw height (Eq. 6b).

Table 3. Critical flaw size results for embedded flaws offset 0.07874 inch (2 mm) from the ID: uniform residual.

Offset Embedded Flaw Uniform Residual Stress = 46.5 ksi					
Elastic-Plastic (Shakedown)		Elastic-Plastic (No Shakedown)		Elastic	
Flaw Height (in.)	Flaw Length (in.)	Flaw Height (in.)	Flaw Length (in.)	Flaw Height (in.)	Flaw Length (in.)
0.39**	0.39	0.38*	0.38	0.40**	0.40
0.37*	0.74	0.36*	0.72	0.40**	0.80
0.36*	1.44	0.28*	1.13	0.38	1.51
0.3b*	1.78	0.27*	1.36	0.36	1.78
0.35*	2.11	0.26*	1.56	0.34	2.05
0.35*	2.81	0.25*	2.01	0.32	2.59
0.35*	3.47	0.24*	2.43	0.31	3.14
0.35*	6.94	0.24*	4.71	0.30	5.95
0.34*	34.32	0.23*	23.15	0.29	28.93
0.35*	69.44	0.23*	46.29	0.29	57.76

* Critical height equals K solution geometrical validity limit based on first order plastically corrected flaw height (Eq. 6).
** Critical height equals K solution geometrical validity limit based on flaw height.(Eq. 6a).

Table 4. Critical flaw size results for surface flaws emanating from the OD: Double-V residual.

Surface OD Flaw Double-V Residual Stress					
Elastic-Plastic (Shakedown)		Elastic-Plastic (No Shakedown)		Elastic	
Flaw Height (in.)	Flaw Length (in.)	Flaw Height (in.)	Flaw Length (in.)	Flaw Height (in.)	Flaw Length (in.)
0.45*	0.45	0.45*	0.45	0.45**	0.45
0.45*	0.90	0.45*	0.90	0.45**	0.90
0.44*	1.75	0.43*	1.73	0.45**	1.80
0.43*	2.14	0.42*	2.11	0.45**	2.25
0.42*	2.51	0.41*	2.43	0.45**	2.70
0.39*	3.10	0.37*	2.99	0.45**	3.60
0.37*	3.69	0.36*	3.55	0.32	3.24
0.32*	6.39	0.31*	6.21	0.27	5.49
0.26	26.18	0.25	25.21	0.25	25.08
0.26	51.27	0.25	49.54	0.25	49.73

* Critical height equals K solution geometrical validity limit based on first order plastically corrected flaw height (Eq. 6b).
** Critical height equals K solution geometrical validity limit based on flaw height (Eq. 6a).

Table 5. Critical flaw size results for embedded center flaws: Double-V residual.

Embedded Center Flaw Double-V Residual Stress					
Elastic-Plastic (Shakedown)		Elastic-Plastic (No Shakedown)		Elastic	
Flaw Height (in.)	Flaw Length (in.)	Flaw Height (in.)	Flaw Length (in.)	Flaw Height (in.)	Flaw Length (in.)
0.45*	0.45	0.45*	0.45	0.45**	0.45
0.43*	0.86	0.43*	0.85	0.45**	0.90
0.41*	1.66	0.41*	1.62	0.45**	1.80
0.41*	2.02	0.40*	2.00	0.45**	2.25
0.41*	2.43	0.40*	2.38	0.45**	2.70
0.40*	3.20	0.39*	3.13	0.45**	3.60
0.40*	3.96	0.39*	3.87	0.45**	4.50
0.39*	7.83	0.38*	7.65	0.45**	9.00
0.39*	38.70	0.38*	38.25	0.45**	45.00
0.39*	77.39	0.38*	76.49	0.45**	90.00

* Critical height equals K solution geometrical validity limit based on first order plastically corrected flaw height (Eq. 6b).
** Critical height equals K solution geometrical validity limit based on flaw height (Eq. 6a).

Table 6. Critical flaw size results for embedded flaws offset 0.07874 inch (2 mm) from the OD: Double-V residual.

Offset Embedded Flaw Double-V Residual Stress					
Elastic-Plastic (Shakedown)		Elastic-Plastic (No Shakedown)		Elastic	
Flaw Height (in.)	Flaw Length (in.)	Flaw Height (in.)	Flaw Length (in.)	Flaw Height (in.)	Flaw Length (in.)
0.40**	0.40	0.40**	0.40	0.40**	0.40
0.40**	0.80	0.40**	0.80	0.40**	0.80
0.40**	1.58	0.39**	1.56	0.40**	1.60
0.40**	1.98	0.39*	1.96	0.40**	2.00
0.39**	2.35	0.39*	2.35	0.40**	2.39
0.39*	3.13	0.39*	3.10	0.40**	3.19
0.39*	3.91	0.39*	3.87	0.40**	3.99
0.39*	7.74	0.38*	7.66	0.40**	7.98
0.39*	38.71	0.38*	38.31	0.40**	39.91
0.39*	77.42	0.38*	76.62	0.40**	79.81

* Critical height equals K solution geometrical validity limit based on first order plastically corrected flaw height (Eq. 6b).
** Critical height equals K solution geometrical validity limit based on flaw height (Eq. 6a).

Table 7. Critical flaw size results for surface flaws emanating from the ID: 7 Pass (ID Last) residual.

Surface ID Flaw 7 Pass (ID Last)									
Elastic-Plastic K_C = 154 ksi inch$^{1/2}$ (Shakedown)		Elastic-Plastic K_C = 154 ksi inch$^{1/2}$ (No Shakedown)		Elastic K_C = 62 ksi inch$^{1/2}$		Elastic-Plastic K_C = 115 ksi inch$^{1/2}$ (No Shakedown)		Elastic-Plastic K_C = 62 ksi inch$^{1/2}$ (No Shakedown)	
Flaw Height (in.)	Flaw Length (in.)	Flaw Height (in.)	Flaw Length (in.)	Flaw Height (in.)	Flaw Length (in.)	Flaw Height (in.)	Flaw Length (in.)	Flaw Height (in.)	Flaw Length (in.)
0.45*	0.45	0.45*	0.45	0.30	0.30	0.45*	0.45	0.18	0.18
0.45*	0.90	0.45*	0.90	0.22	0.44	0.38	0.77	0.16	0.32
0.45*	1.80	0.44*	1.76	0.19	0.76	0.27	1.06	0.13	0.51
0.45*	2.25	0.32*	1.60	0.16	0.81	0.24	1.21	0.12	0.58
0.45*	2.70	0.27*	1.62	0.14	0.86	0.22	1.34	0.11	0.63
0.38*	3.02	0.24*	1.91	0.12	0.99	0.20	1.61	0.09	0.72
0.31*	3.10	0.22*	2.20	0.11	1.14	0.19	1.88	0.08	0.81
0.26*	5.13	0.19*	3.78	0.10	1.96	0.13	2.51	0.06	1.21
0.19	18.64	0.11	11.15	0.09	9.16	0.09	9.39	0.05	5.15
0.18	36.32	0.11	21.69	0.09	18.25	0.09	18.40	0.05	10.23

* Critical height equals K solution geometrical validity limit based on first order plastically corrected flaw height (Eq. 6b).

Table 8. Critical flaw size results for offset embedded flaws: 7 Pass (ID Last) residual.

Offset Embedded Flaw 7 Pass (ID Last)					
Elastic-Plastic (Shakedown)		Elastic-Plastic (No Shakedown)		Elastic	
Flaw Height (in.)	Flaw Length (in.)	Flaw Height (in.)	Flaw Length (in.)	Flaw Height (in.)	Flaw Length (in.)
0.39**	0.39	0.39*	0.39	0.40**	0.40
0.39**	0.77	0.39*	0.77	0.40**	0.80
0.39**	1.55	0.27*	1.09	0.40**	1.60
0.39*	1.94	0.25*	1.24	0.40**	2.00
0.39*	2.32	0.23*	1.39	0.40**	2.39
0.38*	3.06	0.22*	1.76	0.40**	3.19
0.38*	3.83	0.21*	2.12	0.40**	3.99
0.38*	7.66	0.20*	4.07	0.31	6.17
0.38*	38.31	0.20*	19.95	0.28	28.02
0.38*	76.62	0.20*	39.91	0.28	55.77

* Critical height equals K solution geometrical validity limit based on first order plastically corrected flaw height (Eq. 6b).
** Critical height equals K solution geometrical validity limit based on flaw height (Eq. 6a).

Table 9. Critical flaw size results for surface flaws emanating from the OD: 7 Pass (OD Last) residual.

Surface OD Flaw 7 Pass (OD Last)					
Elastic-Plastic (Shakedown)		Elastic-Plastic (No Shakedown)		Elastic	
Flaw Height (in.)	Flaw Length (in.)	Flaw Height (in.)	Flaw Length (in.)	Flaw Height (in.)	Flaw Length (in.)
0.45*	0.45	0.45*	0.45	0.45**	0.45
0.45*	0.90	0.45*	0.90	0.45**	0.90
0.45*	1.80	0.45*	1.78	0.45**	1.80
0.45*	2.23	0.44*	2.20	0.45**	2.25
0.44*	2.65	0.44*	2.62	0.45**	2.70
0.42*	3.35	0.40*	3.17	0.45**	3.60
0.38*	3.82	0.36*	3.60	0.29	2.93
0.30*	6.03	0.29*	5.76	0.23	4.53
0.23	23.13	0.22	21.83	0.21	20.61
0.23	45.08	0.21	42.51	0.20	40.86

* Critical height equals K solution geometrical validity limit based on first order plastically corrected flaw height (Eq. 6b).
** Critical height equals K solution geometrical validity limit based on flaw height (Eq. 6a).

Table 10. Critical flaw size results for embedded center flaws: 7 Pass (OD Last) residual.

Offset Embedded Flaw 7 Pass (OD Last)					
Elastic-Plastic (Shakedown)		Elastic-Plastic (No Shakedown)		Elastic	
Flaw Height (in.)	Flaw Length (in.)	Flaw Height (in.)	Flaw Length (in.)	Flaw Height (in.)	Flaw Length (in.)
0.40**	0.40	0.40**	0.40	0.40**	0.40
0.40**	0.80	0.40**	0.80	0.40**	0.80
0.40**	1.60	0.40**	1.60	0.40**	1.60
0.40**	2.00	0.40**	2.00	0.40**	2.00
0.40**	2.39	0.40*	2.39	0.40**	2.39
0.40**	3.19	0.40*	3.19	0.40**	3.19
0.40**	3.99	0.40*	3.99	0.40**	3.99
0.40*	7.98	0.40*	7.98	0.40**	7.98
0.40*	39.91	0.40*	39.91	0.40**	39.91
0.40*	79.81	0.40*	79.81	0.40**	79.81

* Critical height equals K solution geometrical validity limit based on first order plastically corrected flaw height (Eq. 6b).
** Critical height equals K solution geometrical validity limit based on flaw height (Eq. 6a).

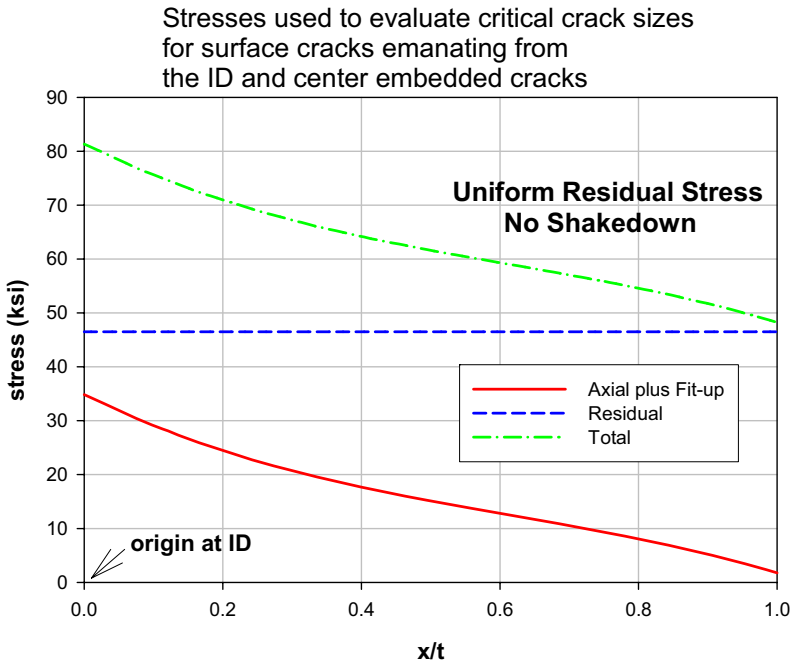

(a)

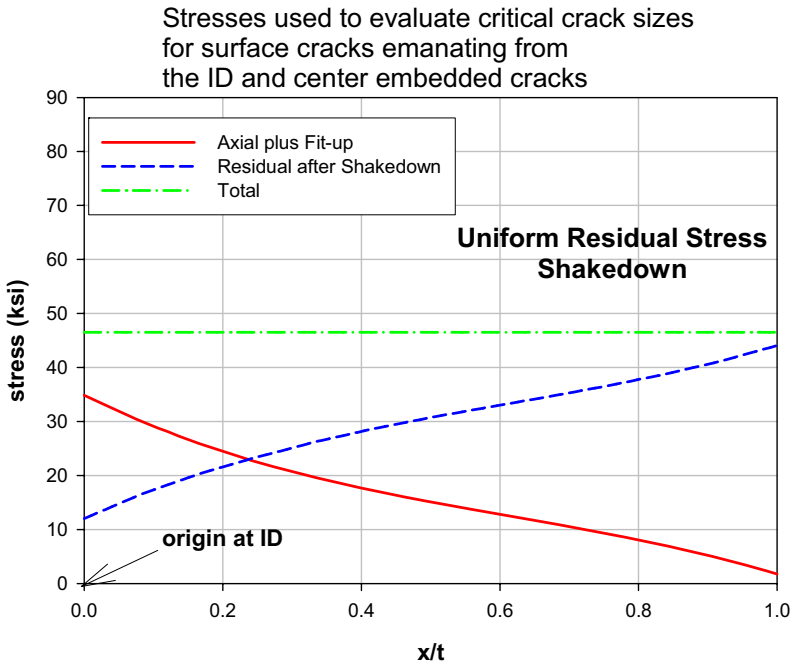

(b)

Figure 2. The effect of shakedown on a uniform residual stress equal to the yield stress. Inset (a) shows the axial and fit-up and residual stresses and the total absent shakedown. Inset (b) shows the same stresses after shakedown has reduced the residual stress due to plastic relaxation.

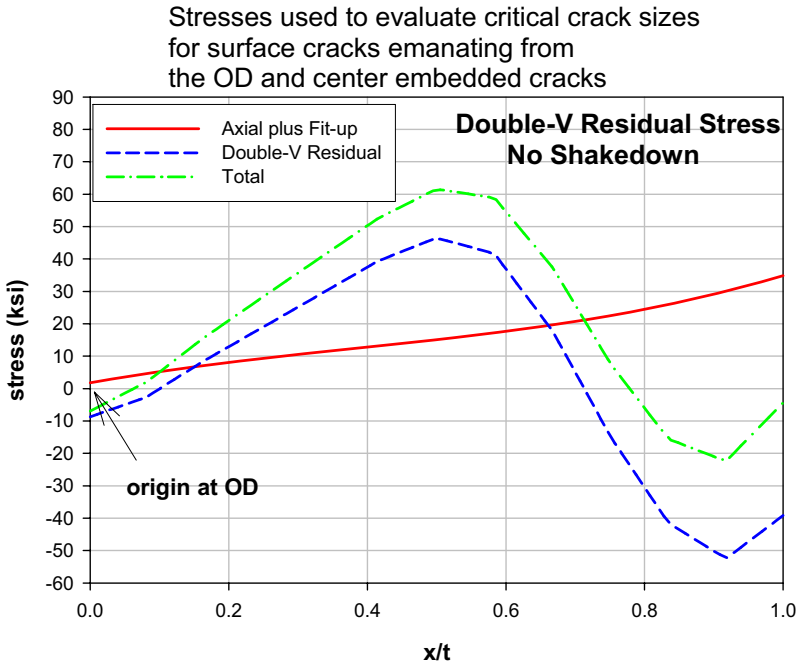

(a)

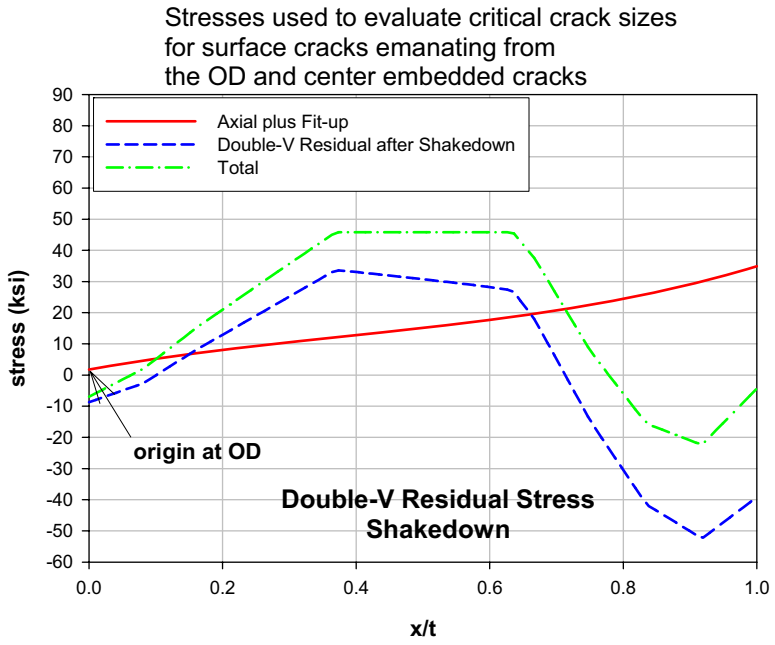

(b)

Figure 3. The effect of shakedown on a variable residual stress (signified as "Double-V") determined from finite element analysis. Inset (a) shows the axial and fit-up and residual stresses and the total absent shakedown. Inset (b) shows the same stresses after shakedown has reduced the residual stress due to plastic relaxation.

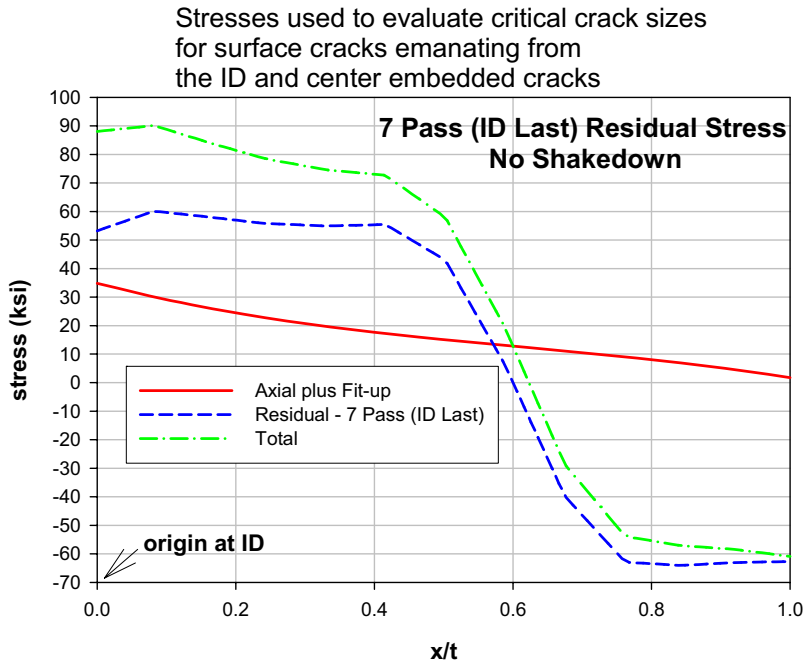

(a)

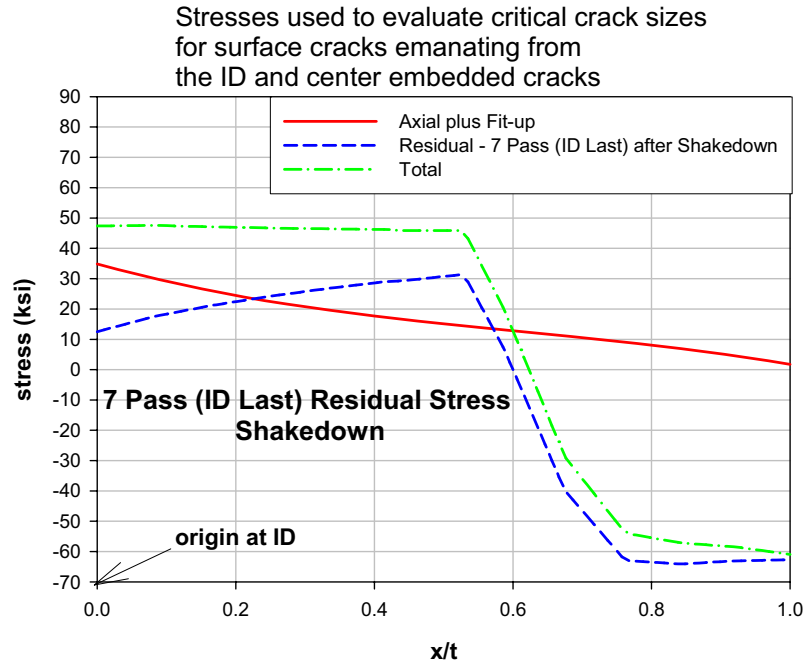

(b)

Figure 4. The effect of shakedown on a variable residual stress (signified as "7 Pass (ID Last")
determined from finite element analysis. Inset (a) shows the axial and fit-up and residual
stresses and the total absent shakedown. Inset (b) shows the same stresses after
shakedown has reduced the residual stress due to plastic relaxation.

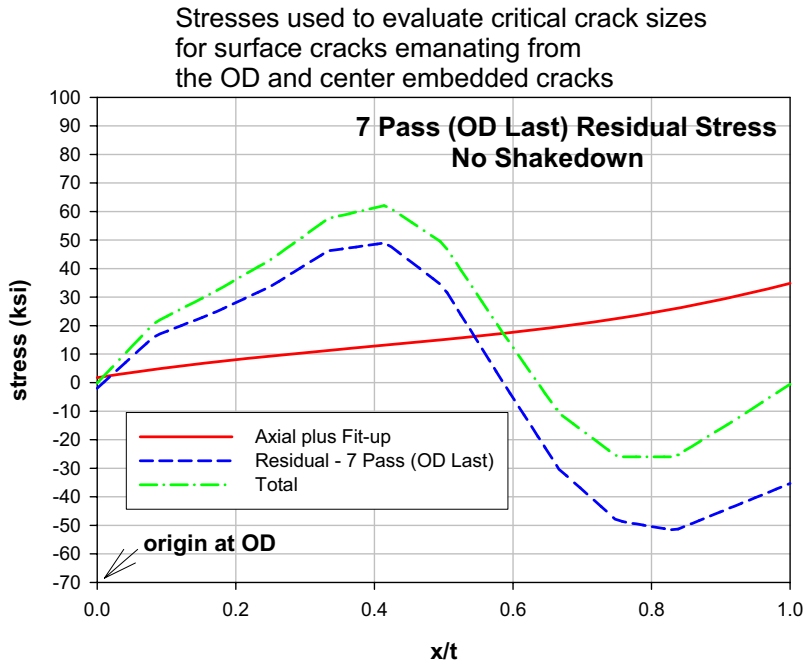

(a)

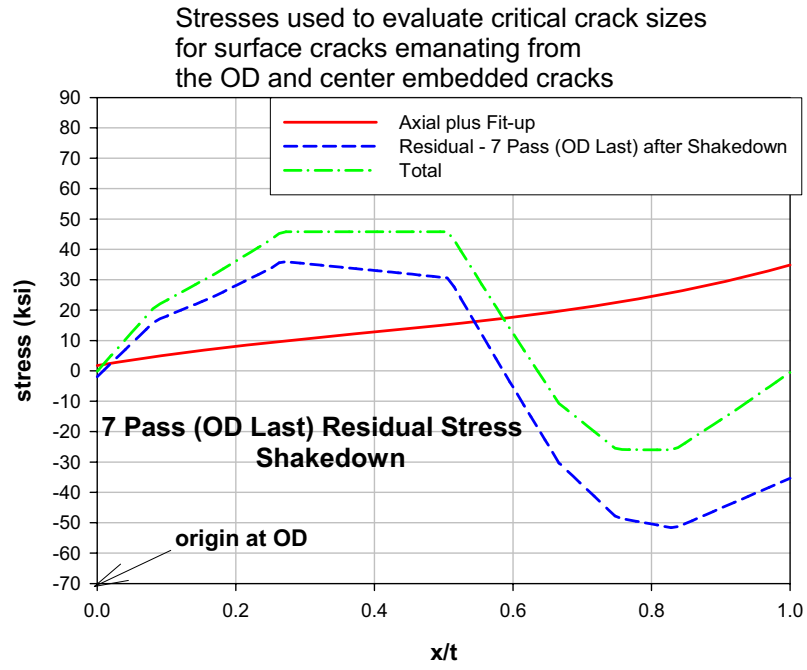

(b)

Figure 5. The effect of shakedown on a variable residual stress (signified as "7 Pass (OD Last")
determined from finite element analysis. Inset (a) shows the axial and fit-up and residual
stresses and the total absent shakedown. Inset (b) shows the same stresses after
shakedown has reduced the residual stress due to plastic relaxation.

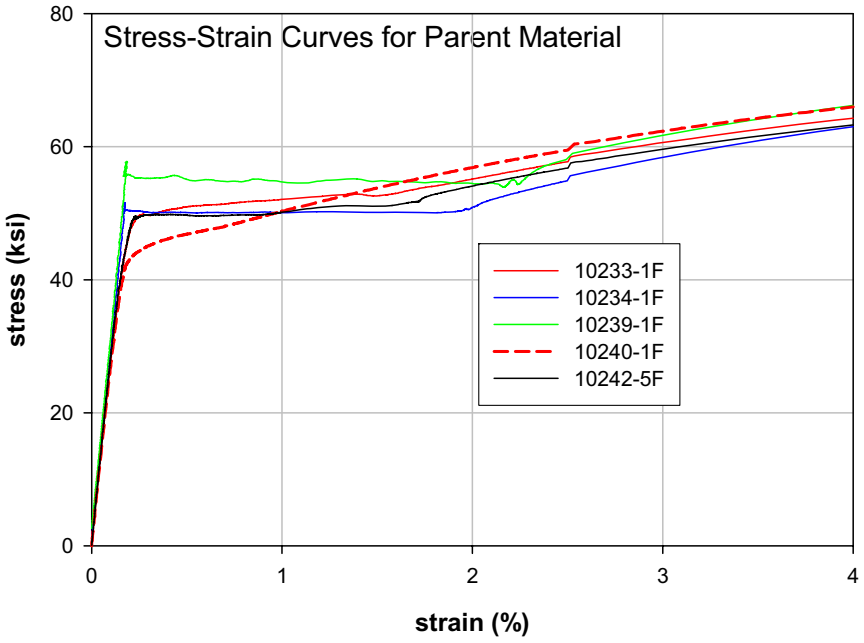

(a)

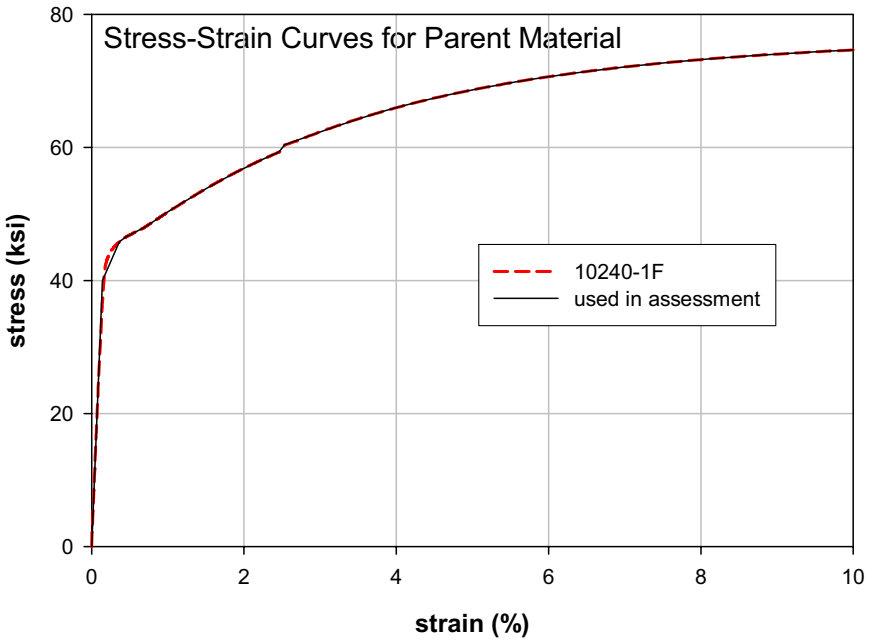

(b)

Figure 6. Inset (a) displays stress-strain curves corresponding to parent material and shows specimen 10240-1F has the lowest yield stress. Inset (b) compares the stress-strain curve for specimen 10240-1F with the curve used in the CFS evaluations.

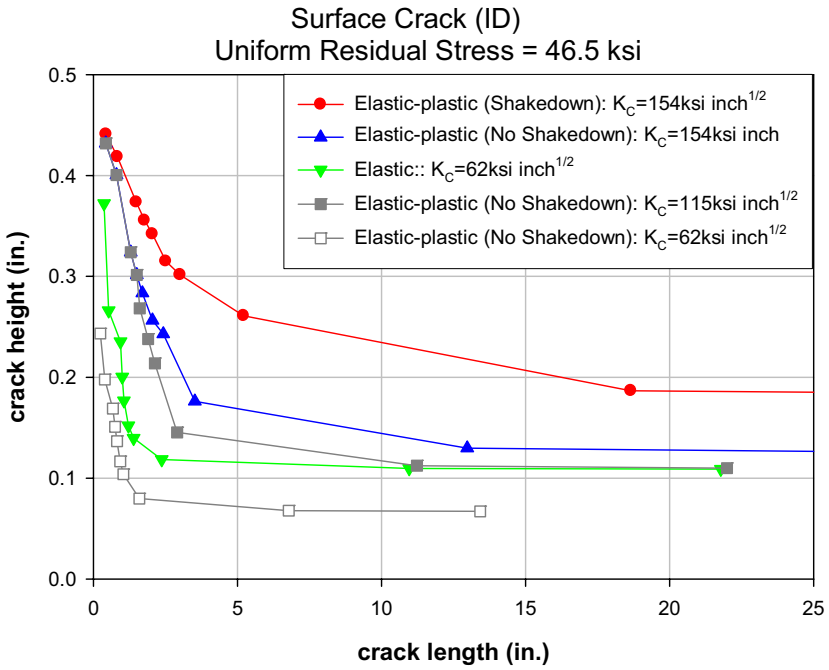

Figure 7. Critical flaw sizes for surface flaws emanating from the ID: uniform residual stress. (Some of the critical sizes are based on non-toughness related criteria – see Table 2.)

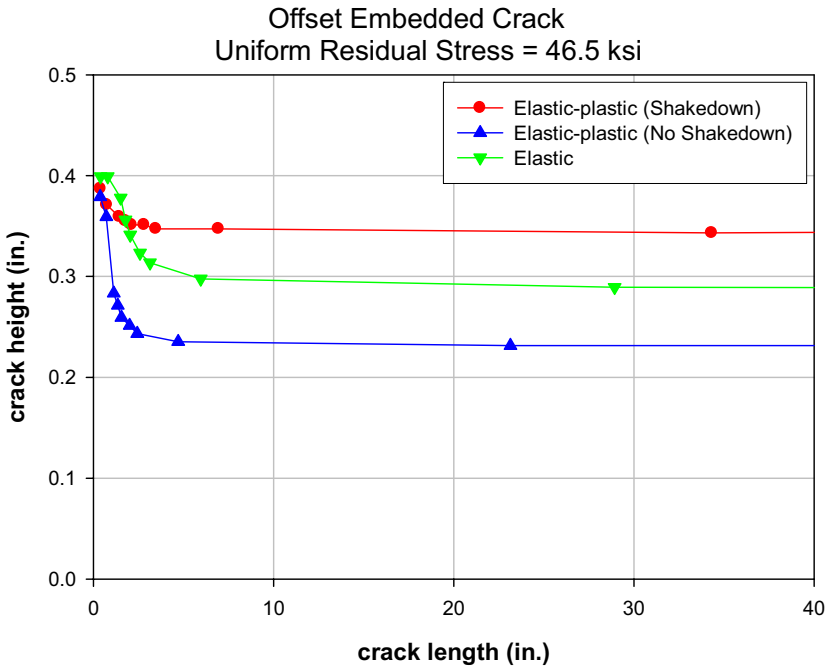

Figure 8. Critical flaw sizes for offset embedded flaws: uniform residual stress. (Some of the critical sizes are based on non-toughness related criteria – see Table 3.)

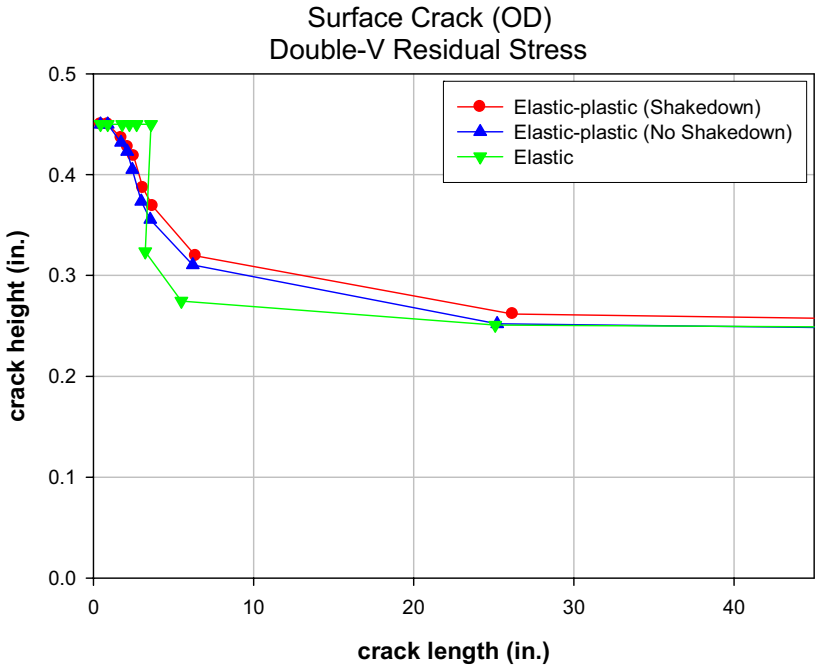

Figure 9. Critical flaw sizes for surface flaws emanating from the OD: Double-V residual stress. (Some of the critical sizes are based on non-toughness related criteria – see Table 4.)

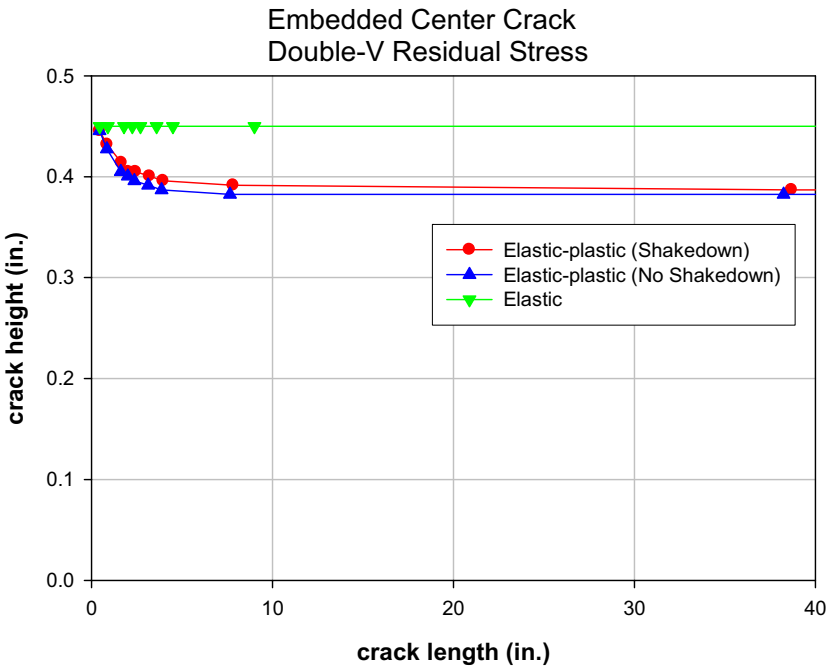

(a) Center Flaw

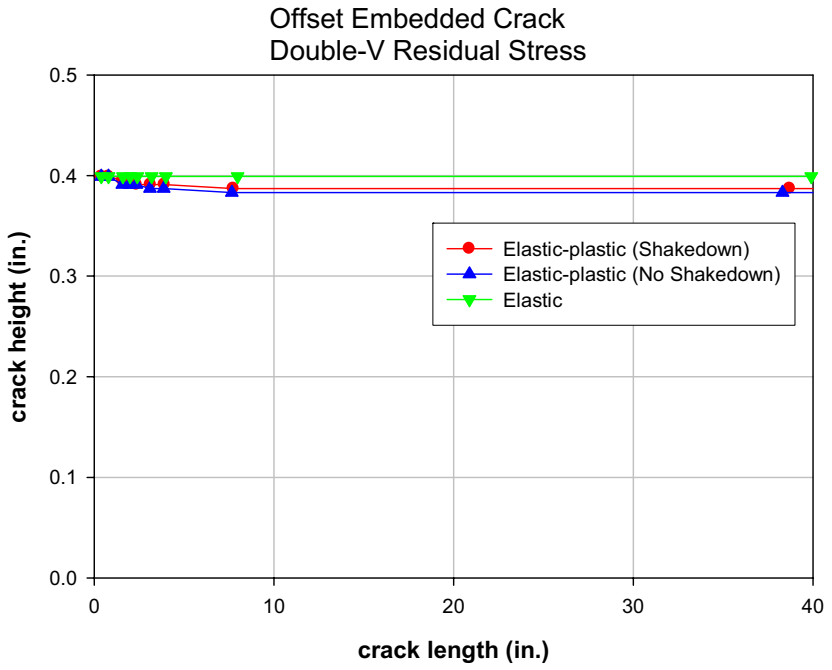

(b) Flaw Offset 0.07874 inch (2 mm) from OD

Figure 10. Critical flaw sizes for center (a) and offset (b) embedded flaws: Double-V residual stress. (Some of the critical sizes are based on non-toughness related criteria – see Tables 5 and 6.)

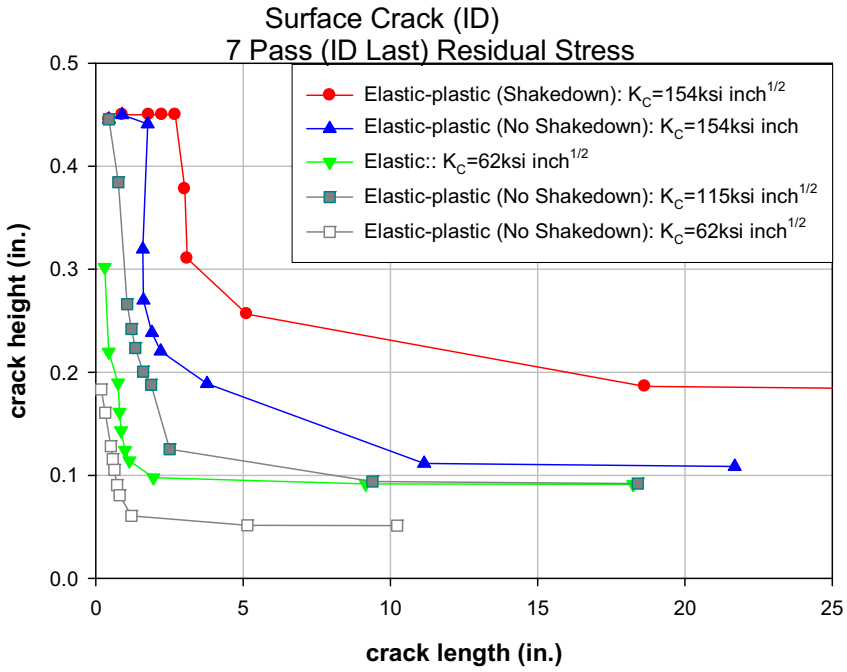

Figure 11. Critical flaw sizes for surface flaws emanating from the ID: 7 Pass (ID Last) residual stress. (Some of the critical sizes are based on non-toughness related criteria – see Table 7.)

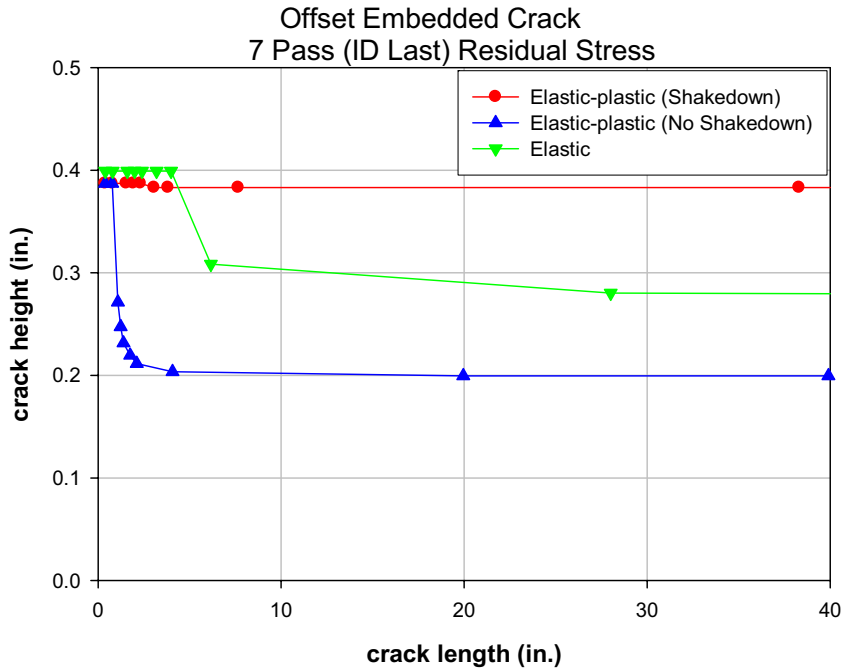

Figure 12. Critical flaw sizes for embedded flaws offset 0.07874 inch (2 mm) from the ID: 7 Pass (ID Last) residual stress. (Some of the critical sizes are based on non-toughness related criteria – see Table 8.)

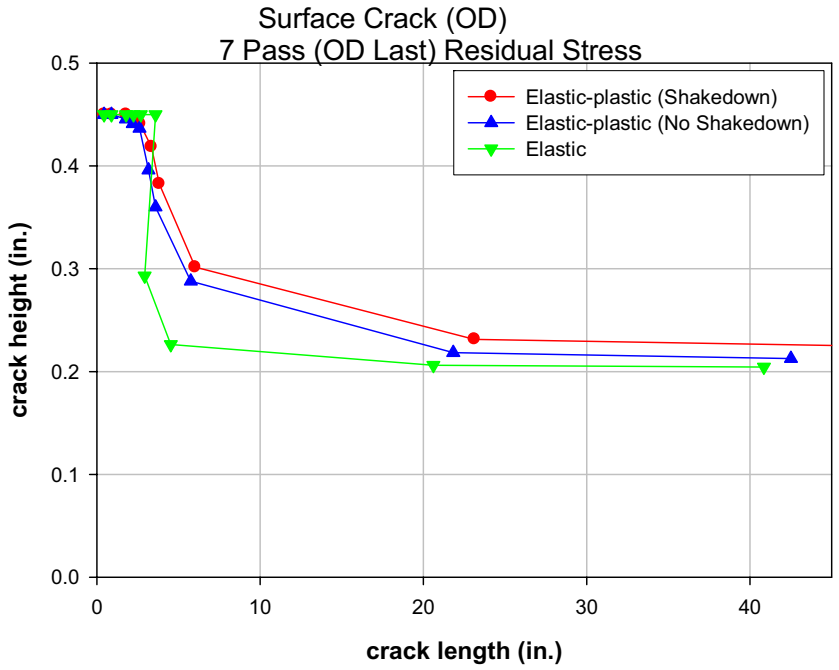

Figure 13. Critical flaw sizes for surface flaws emanating from the OD: 7 Pass (OD Last) residual stress. (Some of the critical sizes are based on non-toughness related criteria – see Table 9.)

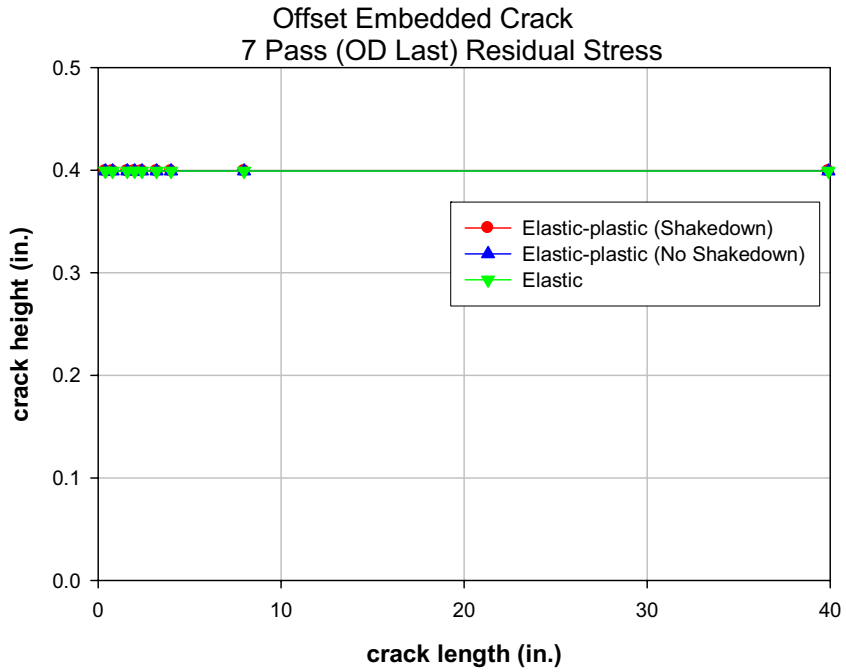

Figure 14. Critical flaw sizes for embedded flaws offset 0.07874 inch (2 mm) from the OD: 7 Pass (OD Last) residual stress. (Some of the critical sizes are based on non-toughness related criteria – see Table 10.)

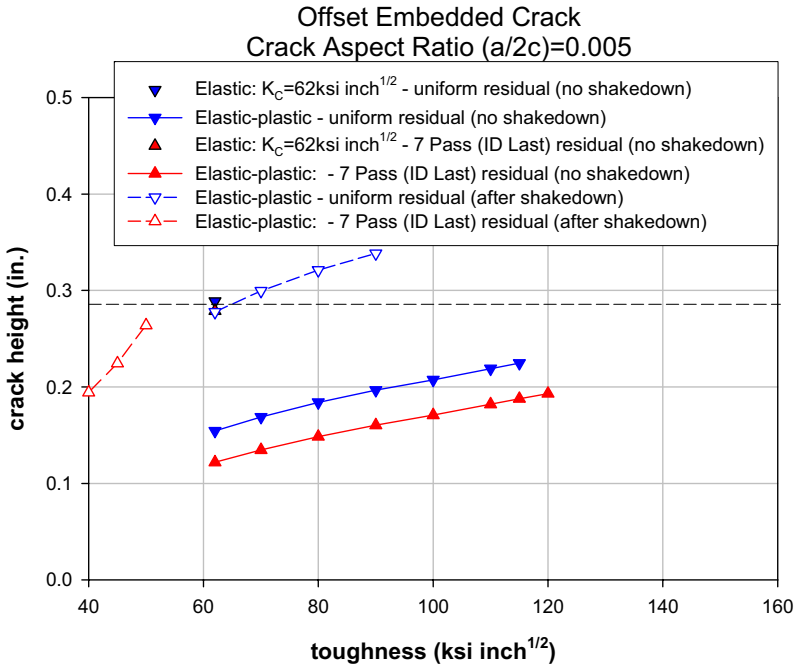

Figure 15. Critical flaw heights (a) for embedded flaws of constant aspect ratio (h/2c) offset 0.07874 inch (2 mm) from the ID as a function of toughness: Uniform and 7 Pass (ID Last) residual stresses.

REPORT DOCUMENTATION PAGE

Form Approved
OMB No. 0704-0188

1. REPORT DATE *(DD-MM-YYYY)*	2. REPORT TYPE	3. DATES COVERED *(From - To)*
01-09-2008	Contractor Report	December 2006 - January 2008

4. TITLE AND SUBTITLE

Elastic-Plastic Fracture Mechanics Analysis
of Critical Flaw Size in ARES I-X Flange-to-Skin Welds

5a. CONTRACT NUMBER
NNL07AA00B

5b. GRANT NUMBER

5c. PROGRAM ELEMENT NUMBER

6. AUTHOR(S)

Chell, G. Graham; and Hudak, Stephen J., Jr.

5d. PROJECT NUMBER

5e. TASK NUMBER

5f. WORK UNIT NUMBER
510505.03.07.01.11

7. PERFORMING ORGANIZATION NAME(S) AND ADDRESS(ES)

NASA Engineering and Safety Center
Langley Research Center
Hampton, VA 23681-2199

8. PERFORMING ORGANIZATION REPORT NUMBER

SwRI Project No. 18.13011
NESC-RP-08-09/06-081-E

9. SPONSORING/MONITORING AGENCY NAME(S) AND ADDRESS(ES)

National Aeronautics and Space Administration
Washington, DC 20546-0001

10. SPONSORING/MONITOR'S ACRONYM(S)
NASA

11. SPONSORING/MONITORING REPORT NUMBER
NASA/CR-2008-215340

12. DISTRIBUTION/AVAILABILITY STATEMENT

Unclassified - Unlimited
Subject Category 39 - Structural Mechanics Availability: NASA CASI (301) 621-0390

13. SUPPLEMENTARY NOTES

NESC Technical Monitor: Ivatury S. Raju

14. ABSTRACT

NASA'sAres 1 Upper Stage Simulator (USS) is being fabricated from welded A516 steel. In order to insure the structural integrity of these welds it is of interest to calculate the critical initial flaw size (CIFS) to establish rational inspection requirements. The CIFS is in turn dependent on the critical final flaw size (CFS), as well as fatigue flaw growth resulting from transportation, handling and service-induced loading. Independent CFS, fatigue flaw growth and CIFS calculations for weld flaws in the flange-to-skin weld of the AersS I USS have been reported in a companion report. These calculations were made using linear elastic fracture mechanics (LEFM), which are thought to be conservative because they are based on a lower bound, so-called "elastic," fracture toughness determined from tests that displayed significant plasticity.

15. SUBJECT TERMS

NESC, CIFS, Ares I-X USS, fracture mechanics, flange-to-skin weld

16. SECURITY CLASSIFICATION OF:			17. LIMITATION OF ABSTRACT	18. NUMBER OF PAGES	19a. NAME OF RESPONSIBLE PERSON
a. REPORT	b. ABSTRACT	c. THIS PAGE			STI Help Desk (email: help@sti.nasa.gov)
U	U	U	UU	40	19b. TELEPHONE NUMBER *(Include area code)* (301) 621-0390